Mechanical Systems and Signal Processing 70-71 (2016) 1117–1130

Contents lists available at ScienceDirect

Mechanical Systems and Signal Processing

journal homepage: www.elsevier.com/locate/ymssp

Step-response of a torsional device with multiple discontinuous non-linearities: Formulation of a vibratory experiment

Michael D. Krak, Jason T. Dreyer, Rajendra Singh *

Acoustics and Dynamics Laboratory, Smart Vehicle Concepts Center, Department of Mechanical and Aerospace Engineering, The Ohio State University, Columbus, OH 43210 USA

ARTICLE INFO

Article history:
Received 18 March 2015
Received in revised form
14 July 2015
Accepted 12 August 2015

Keywords:
Mechanical system dynamics
Signal processing for transient events
Discontinuous stiffness and friction elements
Non-linear dynamics

ABSTRACT

A vehicle clutch damper is intentionally designed to contain multiple discontinuous non-linearities, such as multi-staged springs, clearances, pre-loads, and multi-staged friction elements. The main purpose of this practical torsional device is to transmit a wide range of torque while isolating torsional vibration between an engine and transmission. Improved understanding of the dynamic behavior of the device could be facilitated by laboratory measurement, and thus a refined vibratory experiment is proposed. The experiment is conceptually described as a single degree of freedom non-linear torsional system that is excited by an external step torque. The single torsional inertia (consisting of a shaft and torsion arm) is coupled to ground through parallel production clutch dampers, which are characterized by quasi-static measurements provided by the manufacturer. Other experimental objectives address physical dimensions, system actuation, flexural modes, instrumentation, and signal processing issues. Typical measurements show that the step response of the device is characterized by three distinct non-linear regimes (double-sided impact, single-sided impact, and no-impact). Each regime is directly related to the non-linear features of the device and can be described by peak angular acceleration values. Predictions of a simplified single degree of freedom non-linear model verify that the experiment performs well and as designed. Accordingly, the benchmark measurements could be utilized to validate non-linear models and simulation codes, as well as characterize dynamic parameters of the device including its dissipative properties.

1. Introduction

Practical multi-staged torsional stiffness and friction elements, such as clutch dampers for vehicle drivelines, are designed to transmit variable torque loads while mitigating clearance-induced impact phenomena in gearboxes and other driveline elements [1–7]. Such devices are discontinuously non-linear by nature (intentional or otherwise) as they contain multiple spring and variable friction elements that are spread over several stages depending on the performance requirements of the car or truck powertrain subsystem [1]. Intentional discontinuous non-linear features include clearances, abrupt changes in stiffness, stoppers, pre-load features, and dry friction elements. A typical torque–relative displacement

* Corresponding author. Tel.: +1 614 292 9044.
E-mail address: singh.3@osu.edu (R. Singh).

http://dx.doi.org/10.1016/j.ymssp.2015.08.013
0888-3270/

$(T_D(\theta,\dot{\theta}))$ curve is shown schematically in Fig. 1(a) where stage transitions are denoted by Θ and stages are indexed by Roman numeral subscripts. In this example, $T_D(\theta,\dot{\theta})$ is described by a sum of piecewise elastic torque $T_K(\theta)$ and Coulomb hysteresis amplitude $H(\theta)$ (as shown in Fig. 1(b) and (c)). The drive side (subscript $+$) and coast side (subscript $-$) are often designed to be asymmetric [1,2]. In high load applications, a multi-staged clutch damper may have a torque capacity of the order of 1000 N m and stiffness ratios between adjacent stages might be as high as 100 or 1000.

It is evident that linear models cannot fully describe the dynamics of multi-staged clutch dampers, especially when considering transient phenomena such as driveline clunk [4]. Development of the appropriate non-linear models requires validation through benchmark time-domain measurements that are often not available. Previous articles have analyzed discontinuous non-linear systems mostly by using mathematical or computational models [2–18]; however, few papers use

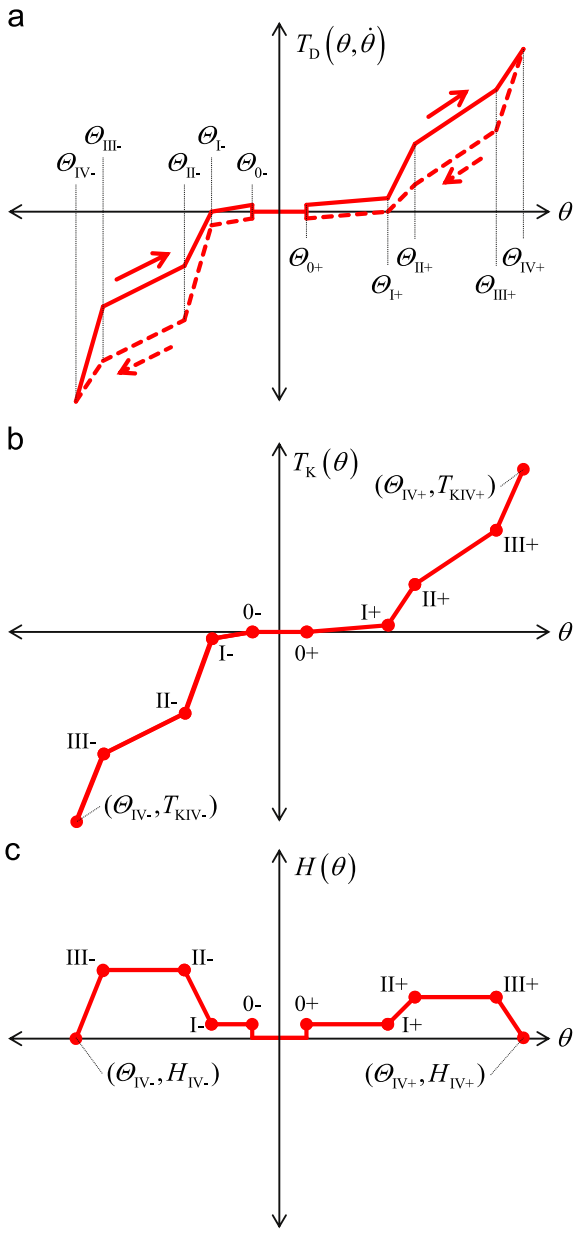

Fig. 1. Typical quasi-static performance curve for a four-stage, asymmetric clutch damper displaying relations for (a) transmitted torque $T_D(\theta,\dot{\theta})$, (b) elastic torque $T_K(\theta)$, and (c). Coulomb hysteresis amplitude $H(\theta)$ where θ and $\dot{\theta}$ are relative angular displacement and velocity. Key: (—) – $\dot{\theta}>0$, (- -) – $\dot{\theta}<0$, K – stiffness, H – Coulomb hysteresis, T – torque, and Θ – stage transition (angular). Stages are denoted by subscripts I, II, III, and IV, clearances by subscript 0, and drive/coast sides by subscripts $+/-$.

experimental methods [2,14–18] and even fewer focus on transient events [2,17,18]. For instance, Gurm et al. [17] proposed a step-response experiment to study the clunk behavior of a two degree of freedom driveline system given a single clearance and dry friction element. Crowther et al. [18] suggested a similar experiment to study the step-response of a multiple degree of freedom driveline system with multiple clearances. Both prior experiments [17,18] considered non-rotating systems that were excited by an external step-like torque provided by a variable mass drop (using magnets); however, neither included multi-staged stiffness or friction elements.

Additionally, characterization of dissipative elements within multi-staged clutch dampers, such as dry friction, is critical to understanding transient phenomena. In particular, dry friction in translational mechanical systems has been a thoroughly investigated topic; see Wojewoda et al. [19] for a review of prior work. Parameter estimation for refined models requires a controlled laboratory experiment that provides accurate measurement of friction force and interfacial velocity, such as the translational system proposed by Wojewoda et al. [19]. However, measurement of these signals in a practical system that utilizes a torsional device is very difficult due to the device's inherent complexity (i.e. known and unknown non-linear features) and limited instrumentation.

Therefore, the chief goal of this article is to propose a refined vibratory (non-rotating) experiment that exhibits the step-response of a torsional device with multi-staged stiffness and friction elements. Additional objectives include the following: 1) discuss and resolve practical mechanical design, instrumentation, and signal processing issues such as system actuation, usage of accelerometers, and time domain analysis; and 2) verify that the experiment is operating as designed by comparing measurements to predictions from a simplified single degree of freedom (SDOF) non-linear model. Characterization of specific dissipative elements within the torsional device will be left to future studies.

2. Problem formulation

The proposed non-rotating experiment is conceptually illustrated in Fig. 2(a). For design purposes the experiment is simply described as a SDOF non-linear torsional system. An inertia element (J consisting of a shaft and torsion arm) is coupled to ground through a shaft spline in series with two parallel practical multi-staged torsional springs of stiffness $K(\theta)$ and Coulomb hysteresis amplitude $H(\theta)$ that are assumed from quasi-static performance curves [5]; also, refer to Appendix A for the identification of symbols. It is assumed that the multi-staged springs and hysteresis elements are identical, synchronous, and have negligible torsional inertia. Additional dissipation sources could be modeled by a viscous damping element (C) located between J and ground; further system modeling and estimation of parameters are discussed later. Specific experimental objectives are established as follows.

1) Select production components, such as multi-staged clutch dampers, clutch assembly, clutch shaft, and flywheel, that provide $K(\theta)$ and $H(\theta)$; the clutch damper must have at least three stages, say I, II and III, where II is a pre-load feature.
2) Select components such that the corresponding linear system (with stiffness $K_{\mathrm{III}+}=(T_{\mathrm{KIII}+}-T_{\mathrm{KII}+})/(\Theta_{\mathrm{III}+}-\Theta_{\mathrm{II}+})$ and torsional inertia J) has a natural period $(\tau_{\mathrm{n}}=2\pi/(K_{\mathrm{III}+}/J)^{0.5})$ of about 100 ms; the step response of most real-world vehicle drivelines is closely related to the torsional surge mode which has a natural frequency between 5 and 15 Hz and is often estimated using a SDOF approximation [12,13,17,18].
3) Select the first relevant flexural mode of the torsion arm to be greater than 100 Hz to ensure minimal interaction with angular motion $\theta(t)$.
4) Excite the system with a step-like torque $T(t)$ that is approximated by a ramp function initiated at $t=0$ with duration t_{e} and is defined by initial (θ_{o}, T_{o}) and final (θ_{f}, T_{f}) operating points of J; the intent here is to ensure a non-linear response by allowing the points to lie on different stages of the clutch dampers that are defined by the following and illustrated in Fig. 2(b) and (c)

$$\theta_{\mathrm{o}}\in\left[\Theta_{\mathrm{II}+},\quad \Theta_{\mathrm{III}+}\right],\quad \theta_{\mathrm{f}}\in\left[\Theta_{0+},\quad \Theta_{\mathrm{II}+}\right], \tag{1a – b}$$

$$T_{\mathrm{o}}\in\left[T_{\mathrm{KII}+},\quad T_{\mathrm{KIII}+}\right],\quad T_{\mathrm{f}}\in\left[0,\quad T_{\mathrm{KII}+}\right]. \tag{2a–b}$$

5) Choose the sampling period (τ_{s}) to be at most 0.1 ms to prevent aliasing of measured signals.
6) Measure velocity by a direct mean to improve the numerical estimation of angular displacement $\theta(t)$ and acceleration $\ddot{\theta}(t)$.

3. Physical design of the non-linear experiment

The proposed non-rotating experiment is illustrated in Fig. 3 where the flywheel is grounded to a massive steel structure and bed plate for the sake of simplicity. The clutch assembly is bolted to the flywheel and the clutch is engaged (i.e. no slip between the flywheel and clutch dampers). The clutch assembly houses a greased sleeve bearing and two parallel multi-staged clutch dampers. The clutch shaft contacts the two clutch dampers through a spline and is radially supported by the sleeve bearing and an additional ball bearing.

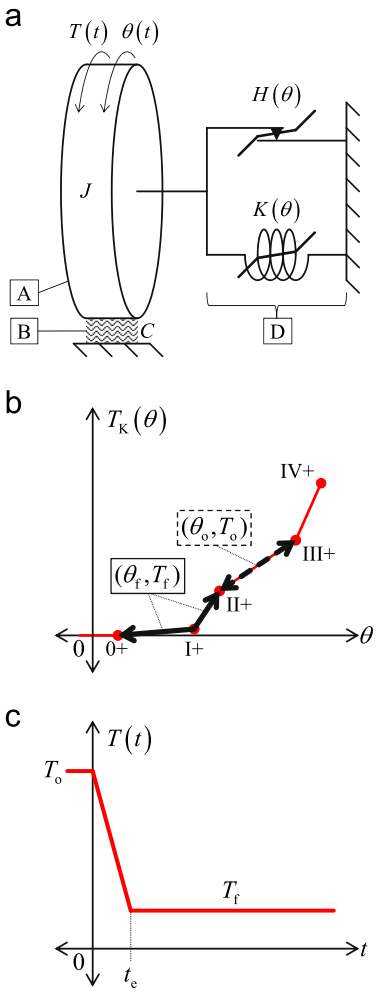

Fig. 2. Conceptual illustration of the proposed non-linear experiment and excitation: (a) SDOF non-linear system, (b) system operating points on the clutch damper performance curve, and (c) $T(t)$ in time domain. Key: A – torsion arm and shaft inertia J, B – viscous damping C, D – two parallel multi-staged clutch dampers of stiffness $K(\theta)$ and Coulomb hysteresis $H(\theta)$.

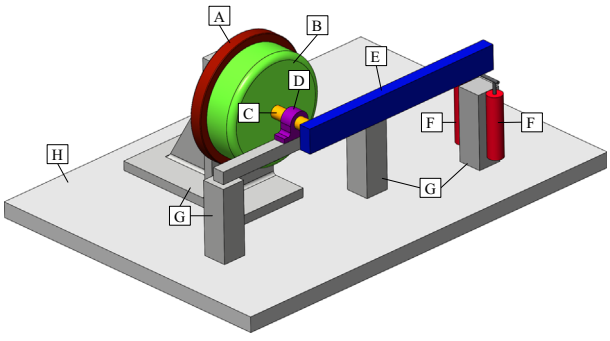

Fig. 3. Physical display of the proposed non-linear experiment (using solid model). Key: A – flywheel (ground), B – clutch assembly (sleeve bearing and two parallel multi-stage clutch dampers), C – clutch shaft, D – ball bearing, E – torsion arm, F – pneumatic cylinders with a mechanical quick release, G – steel support structures (ground), H – steel bed plate (ground).

A torsion arm is rigidly attached to the clutch shaft like previous experiments [17,18]. This arm is relevant to three design objectives: natural frequency, structural modes, and T_f. For simplicity, the torsion arm is constructed of bar stock of length L_x, height L_y, width L_z, and density ρ_A, as illustrated in Fig. 4(a). The effective length (L_A) of the torsion arm is measured from the

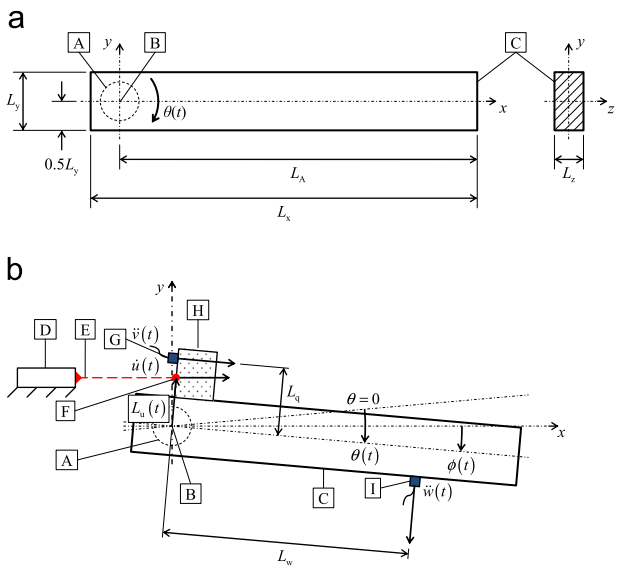

Fig. 4. Illustrations of the torsion arm and measurement of angular motion using a laser vibrometer and accelerometers: (a) torsion arm geometry and (b) instrumentation schematic. Key: A – shaft, B – shaft axis, C – torsion arm, D – laser vibrometer, E – laser, F – laser point, G – translational accelerometer V, H – finished block, and I – translational accelerometer W.

shaft axis to the free end of the arm. The torsion arm's mass moment of inertia about the shaft axis (J_A) is defined as follows:

$$J_A = \rho_A L_x L_y L_z \left(L_x^2/3 + L_y^2/12 + L_A^2 - L_A L_x\right). \tag{3}$$

Inertia J_A must also satisfy the following relation where J_B is the mass moment of inertia of the shaft about its axis and $\tau_n = 100$ ms

$$J_A = K_{III+}(\tau_n/2\pi)^2 - J_B. \tag{4}$$

Torque T_f is equivalent to the torque due to the overhanging mass of the torsion arm (T_A), which is defined as the following where g is the gravitational acceleration; the limits of T_A are determined by Eq. (2b).

$$T_A = 0.5 g \rho_A L_A^2 L_y L_z. \tag{5}$$

The first flexural vibration mode of the torsion arm (within the plane of rotation) must occur beyond 10 ms. To estimate this, the torsion arm is approximated as a beam with fixed (shaft end) and free (load end) boundaries. The beam, with length L_A, height L_y, width L_z, density ρ_A, and modulus of elasticity E_A, is assumed to be nearly slender ($L_y/L_A \approx 0.1$). The rth natural period (τ_{nr}) is defined using Euler–Bernoulli beam theory by the following where β_r is the rth wave number [20]

$$\tau_{nr} = 2\pi / \left[\beta_r^2 \left(E_A L_y^2/12\rho_A\right)^{0.5}\right]. \tag{6}$$

For the first mode ($r=1$), the wave number is $\beta_1 \approx 1.875$. Using Eqs. (2b)–(6), material and geometry of the torsion arm are selected to satisfy the natural period, flexural modes, and T_f.

Torque T_o is the sum of T_A and external torque T_e, where torque T_A is assumed to be constant with respect to θ due to small angular displacements. In previous experiments [17,18], T_e is applied through a variable electromagnet mass drop. The employment of that same method for the current experiment would require a mass drop of approximately 300 kg, which presents significant difficulties. First, it would be unsafe to lift and suddenly drop a large mass. Second, a large electromagnet would have to be attached to the torsion arm, which would lower the first flexural frequency of the arm. Increasing the length of the torsion arm could reduce the drop mass and size of an electromagnet, but spatial restrictions prevent a longer arm. To overcome these issues, T_e is provided by a pair of pneumatic cylinders with a mechanical quick release as shown in Fig. 3.

The pneumatic cylinders are characterized by effective diameter (d) and translational throw (l) and are loaded by gauge pressure (p). Using the upper limit defined by Eq. (1a) and given L_A, the following requirement is defined for l

$$l > 2L_A \sin(\Theta_{III+}). \tag{7}$$

Torque T_e is defined by the following

$$T_e = 0.5\pi d^2 p L_A. \tag{8}$$

Using Eq. (2a) and correcting for T_A, the range of T_e is as follows:

$$T_e \in \left[T_{KII+} - T_A, \quad T_{KIII+} - T_A \right]. \tag{9}$$

The gauge pressure (p_{max}) needed to achieve the upper limit of T_e is found from

$$p_{max} = 2(T_{KIII+} - T_A)/\left(\pi d^2 L_A\right). \tag{10}$$

For the use of shop air, p_{max} must be less than 690 kPa. Using Eqs. (7)–(10) and given L_A and T_A, d and l are selected to meet $(\theta_o, T_o)$and p_{max}.

4. Instrumentation system and signal processing

Previous experiments in the literature [17,18] directly measured acceleration and strain; velocities were estimated by numerically integrating acceleration signals, and strain was considered analogous to displacement [17,18]. However, in the current study $\theta(t)$ and $\ddot{\theta}(t)$, which are difficult to measure directly, are of interest. It is not possible to place sensors (e.g. angular accelerometers, rotary encoders, strain gages) on the clutch shaft due to spatial restrictions. Translational acceleration of the torsion arm can however be directly measured, but this presents several undesirable issues: 1) the impulsive nature of the response would induce "ringing" in the signals [21]; 2) fidelity of the estimated displacements would be reduced by multiple integrations of measured acceleration signals; and 3) accuracy of the accelerometers would diminish when measuring small time-scale dynamics [21], such as those induced by impacts [17,18]. To overcome these complications, a laser vibrometer [22] is chosen to directly measure the translational velocity of a point on the torsion arm. The vibrometer [22] and its paired data acquisition system [23] can sample at a minimum period (τ_s) of 1 μs and measure translational velocities up to 10 m/s; also, refer to Appendix B for the specifications of the instrumentation system. To quantify the error of the vibrometer system [22,23], the velocity of a harmonic shaker is measured without using a filter. The shaker is calibrated to provide 9.81 m/s^2 RMS acceleration at a frequency of 159.2 Hz [24], which corresponds to a 27.7 m/s^2 peak-to-peak acceleration and 2.77 cm/s peak-to-peak velocity. The error of measured peak-to-peak velocity for selected values of τ_s is shown in Table 1; for 3.9 μs $\leq \tau_s \leq$ 1 ms the average error is 6.7%. Acceleration is then calculated by numerically differentiating the velocity signal using forward and central difference methods; the error is 125% at τ_s=3.9 μs and ± 10% at τ_s=1.0 ms. It is assumed that signal noise is prominent at small values of τ_s. Since the truly impulsive nature of the torsional system response is not the primary focus of this study, a very small value of τ_s is not necessary. Therefore, a sampling period of 0.781 ms is chosen to ensure accurate estimation of acceleration and to reduce aliasing.

For measurement of the system response, the laser vibrometer is located a sufficient distance from the experiment to mitigate ground-transmitted vibrations. A clean, flat, reflective surface for the laser point is provided by a square, finished block of negligible torsional inertia; the block is rigidly mounted to the top of the torsion arm such that the measurement surface is in-plane with the shaft axis, as illustrated in Fig. 4(b). The translational velocity of the laser point is denoted by $\dot{u}(t)$, the radial distance from the shaft axis to the laser point by $L_u(t)$, and the angular displacement of the torsion arm with respect to the x-axis by $\phi(t)$. For the purpose of comparison, two translational accelerometers [25], say V and W, are located on the block and torsion arm; the radial distances from the shaft axis to V and W are denoted by L_v and L_w, respectively. Measured translational accelerations $\ddot{v}(t)$ and $\ddot{w}(t)$ are assumed to be tangential to the angular motion of the arm.

Prior to excitation, ϕ_o and L_{uo} are measured with a digital level [26] and a ruler, respectively; u_o is calculated from $u_o = L_{uo} \sin(\phi_o)$. Near $t \approx 0$, the step-like torque is applied to J and measurement is triggered by a 98.1 m/s^2 falling value of $\ddot{w}(t)$; this triggering value is empirically determined and is valid over the range of (θ_o, T_o). The pre- and post-triggering periods are approximately 100 and 4000 ms, respectively. The measured response is contained within the first 1–2 s of the signal, and the latter 2 s provides corrections for numerical integration and quantification of signal noise. After the system reaches equilibrium, ϕ_f is measured using the digital level [26]. Translational displacement $u(t)$ is calculated by numerically integrating signal $\dot{u}(t)$, and $\theta(t)$ is then calculated by the following where θ_f is determined from the static balance of T_f

$$L_u(t) = \left[L_{uo}^2 + (u_o - u(t))^2 - 2L_{uo}(u_o - u(t)) \sin(\phi_o) \right]^{0.5}, \tag{11}$$

Table 1
Sampling errors in peak-to-peak velocity (measured) and acceleration (calculated) for laser vibrometer measurement of a harmonic shaker.

τ_s (ms)	Peak-to-peak velocity error (%)	Peak-to-peak acceleration error	
		Forward difference method (%)	Central difference method (%)
0.0039	7.3	126	125
0.0156	7.2	122	114
0.0625	6.7	88	58
0.2500	6.6	35	24
1.0000	5.8	8.0	−11

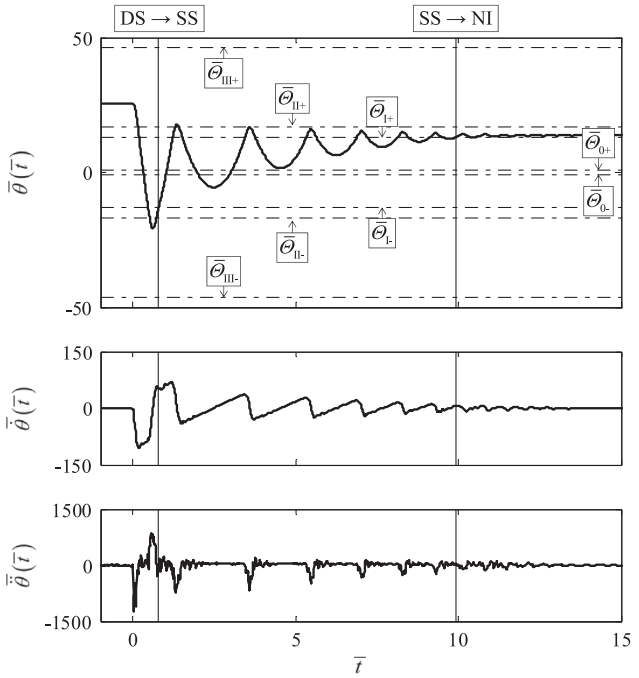

Fig. 5. Normalized measured motions for $\bar{\theta}_o \approx 26$ and demonstration of non-linear response regimes (with dual clutch damper configuration). Key: (—) – measured motion, (|) – regime transition, (– • –) – stage and clearance transitions, DS – double-sided impact regime, SS – single-sided impact regime, NI – no impact regime.

$$\theta(t) = \theta_f + \phi_o - \phi_f - \sin^{-1}\left(\frac{(u_o - u(t))\cos(\phi_o)}{L_u(t)}\right). \tag{12}$$

Angular velocity $\dot{\theta}(t)$, acceleration $\ddot{\theta}(t)$, and jerk $\dddot{\theta}(t)$ are then calculated by numerically differentiating $\theta(t)$ by a forward differencing method. Angular accelerations estimated from signals $\ddot{v}(t)$ and $\ddot{w}(t)$ are defined by the following

$$\ddot{\theta}_v(t) = \ddot{v}(t)/L_v, \quad \ddot{\theta}_w(t) = \ddot{w}(t)/L_w\,. \tag{13a – b}$$

All angular motion signals are then synchronized such that $\left|\ddot{\theta}(0)\right|$ is maximum.

For this experiment, signal analysis in the frequency domain is hindered by the inherently non-linear and transient nature of the responses [27]. Time–frequency domain analysis (though not included in the article) shows that the responses are dominated by lower frequencies, which is evident from the time history alone. Auto and cross-correlations do not provide significant insight due to a very short duration of the response and close spatial proximity of measurement locations [28]. Accordingly, all signals are examined solely in time domain. It is consistent with literature [2–6,12,13,17,18] where the step responses of highly non-linear systems have been studied primarily in time domain.

5. Analysis of measured motions

Typical responses measured by the laser vibrometer (with dual clutch damper configuration) are shown in Fig. 5; all motions and time are normalized as follows to highlight the generic nature of a non-linear device

$$\bar{t} = t/\tau_n, \quad \bar{\theta}(\bar{t}) = \theta(\bar{t})/\Theta_{0+}, \quad \dot{\bar{\theta}}(\bar{t}) = \dot{\theta}(\bar{t})\tau_n/\Theta_{0+}, \quad \ddot{\bar{\theta}}(\bar{t}) = \ddot{\theta}(\bar{t})\tau_n^2/\Theta_{0+}\,. \tag{14a – d}$$

Upon inspection, it can be seen that $\bar{\theta}_o$ and $\bar{\theta}_f$ lie within the desired clutch damper stages. It is also evident that there are three distinct non-linear response regimes: double-sided impact (DS), single-sided impact (SS), and no impact (NI) [29]. The DS regime ($0 < \bar{t} < 0.8$) is characterized by J losing and regaining contact with stage II on both the drive and coast sides at $\bar{\Theta}_{I-}$ and $\bar{\Theta}_{I+}$ with significant peak positive and negative $\ddot{\bar{\theta}}(\bar{t})$. The SS regime ($0.8 < \bar{t} < 10$) is characterized by J losing and regaining contact with stage II on the drive side at $\bar{\Theta}_{I+}$ with significant peak negative $\ddot{\bar{\theta}}(\bar{t})$ only. In the NI regime ($\bar{t} > 10$), J maintains contact with stage II on the drive side ($\bar{\Theta}_{I+} \le \bar{\theta}(\bar{t}) \le \bar{\Theta}_{II+}$); the response remains non-linear and appears nearly harmonic. For this measured response, the time of transition from DS to SS is defined by the last $\bar{t}$ at which $\bar{\theta}(\bar{t}) \le \bar{\Theta}_{I-}$ and from SS to NI by the last $\bar{t}$ at which $\bar{\theta}(\bar{t}) \le \bar{\Theta}_{I+}$.

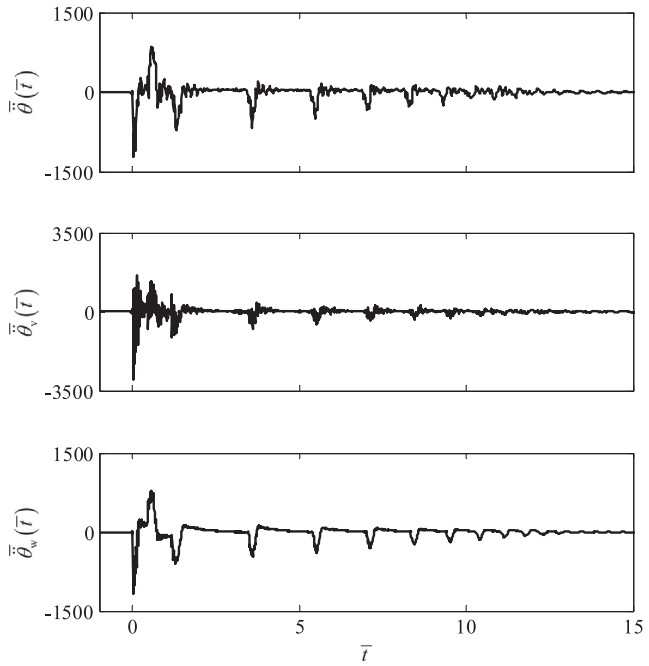

Fig. 6. Comparison of acceleration measurements of $\ddot{\bar{\theta}}(\bar{t})$ from laser vibrometer, $\ddot{\bar{\theta}}_v(\bar{t})$ from accelerometer V, and $\ddot{\bar{\theta}}_w(\bar{t})$ from accelerometer W for $\bar{\theta}_o \approx 26$ (with dual clutch damper configuration). Key: (——) – measured motion.

Table 2
Mean (μ) and standard deviation (σ) of peak-to-peak $\ddot{\bar{\theta}}(\bar{t})$ of the measured responses for $\bar{\theta}_o \approx 26$ over three assemblies (with dual clutch damper configuration).

Measurement set	Peak-to-peak $\ddot{\bar{\theta}}(\bar{t})$ ($\mu \pm \sigma$) for period					
	1	2	3	4	5	6
ASM1	2230 ± 91	991 ± 9	812 ± 59	875 ± 9	690 ± 43	464 ± 19
ASM2	2040 ± 113	986 ± 27	741 ± 48	678 ± 37	578 ± 20	490 ± 28
ASM3	2070 ± 39	943 ± 35	867 ± 11	656 ± 14	514 ± 21	428 ± 13
Overall	2110 ± 123	933 ± 34	807 ± 68	736 ± 14	594 ± 79	461 ± 33

Table 3
Analysis of measurements in terms of the mean (μ) and standard deviation (σ) of response regime transition times and relative displacement between initial and final operating points for $\bar{\theta}_o \approx 26$ over three assemblies (with dual clutch damper configuration).

Measurement set	Response regime transition times ($\mu \pm \sigma$)		Relative displacement between initial and final operating points (μ)	
	$\bar{t}$(DS→SS)	$\bar{t}$(SS→NI)	$\bar{\phi}_o - \bar{\phi}_f$ (Tolerance: ± 0.4)	$\bar{\theta}_o - \bar{\theta}_f$
ASM1	1.61 ± 0.98	13.8 ± 0.06	11.6	11.9
ASM2	0.76 ± 0.01	11.1 ± 0.18	11.6	11.8
ASM3	0.78 ± 0.01	10.3 ± 0.43	11.3	11.7
Overall	1.05 ± 0.66	11.7 ± 1.58	11.5	11.8

Signal $\ddot{\bar{\theta}}(\bar{t})$ from the laser vibrometer is verified by comparing it to $\ddot{\bar{\theta}}_v(\bar{t})$ and $\ddot{\bar{\theta}}_w(\bar{t})$ from accelerometers V and W, all of which are shown in Fig. 6. Peak locations and peak-to-peak amplitudes roughly agree across all signals, which gives confidence in $\ddot{\bar{\theta}}(\bar{t})$. The "ringing" phenomena is clearly present in accelerometer signal $\ddot{\bar{\theta}}_v(\bar{t})$ but nearly absent in $\ddot{\bar{\theta}}_w(\bar{t})$. The close proximity of accelerometer V (point G in Fig. 4(b)) to impact locations and the complex structures of the production

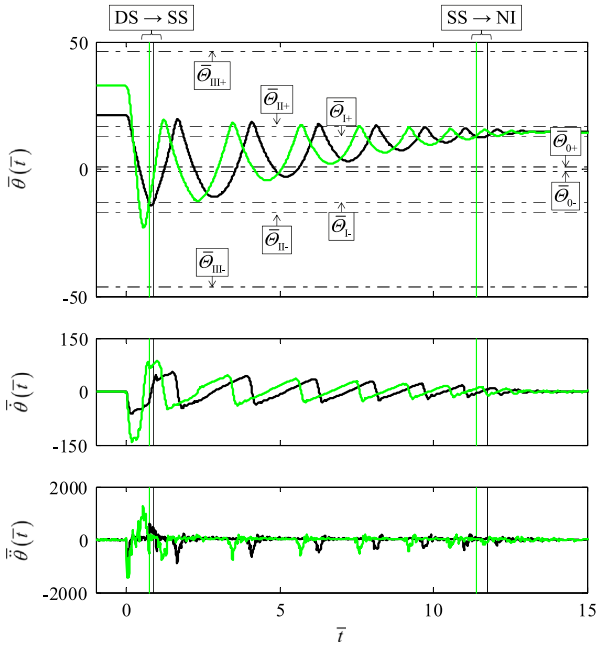

Fig. 7. Comparison of normalized measured motions for $\bar{\theta}_o \approx 21$ and $\bar{\theta}_o \approx 33$, and demonstration of non-linear response regimes (with dual clutch damper configuration). Key: (——) – measured motion for $\bar{\theta}_o \approx 21$, (|) – measured motion for $\bar{\theta}_o \approx 33$, (|) – response regime transition for $\bar{\theta}_o \approx 21$, (——) – response regime transition for $\bar{\theta}_o \approx 33$, (– • –) – stage transitions.

components makes it more susceptible to higher frequency dynamics, whereas accelerometer W (point I in Fig. 4(b)) is located near the free end of the torsion arm.

To demonstrate the repeatability and quantify variance of measurements, 12 response sets are recorded, and metrics are compared. The experiment (with dual clutch damper configuration) is partially disassembled and re-assembled three times, designated ASM1, ASM2, and ASM3. Four measurements per assembly are recorded under similar loading conditions ($\bar{\theta}_o \approx 26$). The arithmetic mean ($\mu$) and standard deviation (σ) of regime transition times and peak-to-peak $\ddot{\bar{\theta}}(\bar{t})$ are calculated for each assembly and all 12 measurements; these are listed in Tables 2 and 3. The peak-to-peak $\ddot{\bar{\theta}}(\bar{t})$ is fairly consistent within each assembly and overall. However, the response regime transition times show more variation, which is most likely due to small differences in shaft alignment (friction) and system actuation. Additionally, the calculation of $\bar{\theta}(\bar{t})$ is verified by comparing $\bar{\theta}_o - \bar{\theta}_f$ to the measured values $\bar{\phi}_o - \bar{\phi}_f$ (tolerance: ± 0.4) as shown in Table 3; all values of $\bar{\theta}_o - \bar{\theta}_f$ fall within the tolerance of $\bar{\phi}_o - \bar{\phi}_f$.

The responses to other loading conditions are also measured; Fig. 7 shows the typical measured responses for $\bar{\theta}_o \approx 21$ and $\bar{\theta}_o \approx 33$. These responses are qualitatively similar to the previous loading condition ($\bar{\theta}_o \approx 26$, Fig. 5). All responses have the desired initial and final operating points and distinct non-linear regimes (DS, SS, and NI). The regime transition times and peak-to-peak $\ddot{\bar{\theta}}(\bar{t})$ are very similar; however there is a significant difference for the DS regime. As the amplitude of T_o increases, the peak-to-peak value of $\ddot{\bar{\theta}}(\bar{t})$ in the DS regime also increases and peak values of $\ddot{\bar{\theta}}(\bar{t})$ occur earlier for all regimes.

6. Development of a simple non-linear dynamic model

The experiment is first simplified by adjusting the position of the shaft so that it contacts only one of the two clutch dampers. This overcomes complexities due to asynchronous contact and misalignment between the clutch dampers and the shaft. The step-like response of the single clutch damper configuration is measured using the previously described procedures. To verify that the measured motions are representative of the designed system, comparisons are made to the predictions from a simplified SDOF non-linear model. The experiment is described by the following equation of motion corresponding to Fig. 2, where it is assumed that all dissipation sources are lumped into a single viscous element C, and the dry friction is ignored for the sake of simplicity

$$J\ddot{\theta}(t) + C\dot{\theta}(t) + T_D\left(\theta, \dot{\theta}\right) = T(t). \tag{15}$$

The non-linear function $T_D(\theta, \dot{\theta})$ is the torque transmitted to J through the spline clearance in series with the clutch damper

and is the sum of elastic and hysteretic torques

$$T_{\mathrm{D}}\left(\theta,\dot{\theta}\right)=T_{\mathrm{K}}(\theta)+H(\theta)\Psi\left(\dot{\theta}\right). \tag{16}$$

The elastic torque $T_{\mathrm{K}}(\theta)$ is defined as the following where $\Xi(\theta)=0.5(\mathrm{sgn}(\theta)+1)$

$$\begin{aligned}T_{\mathrm{K}}(\theta)=\sum_{\mathrm{j=I}}^{\mathrm{N}}\Bigg\{&\left[T_{\mathrm{K(j-I)+}}+\left(\frac{T_{\mathrm{Kj+}}-T_{\mathrm{K(j-I)+}}}{\Theta_{\mathrm{j+}}-\Theta_{\mathrm{(j-I)+}}}\right)(\theta-\Theta_{\mathrm{(j-I)+}})\right]\left[\Xi(\theta-\Theta_{\mathrm{(j-I)+}})-\Xi(\theta-\Theta_{\mathrm{j+}})\right]\\&+\ldots\left[T_{\mathrm{K(j-I)-}}+\left(\frac{T_{\mathrm{K(j-I)-}}-T_{\mathrm{Kj-}}}{\Theta_{\mathrm{(j-I)-}}-\Theta_{\mathrm{j-}}}\right)(\theta-\Theta_{\mathrm{(j-I)-}})\right]\left[\Xi(\theta-\Theta_{\mathrm{j-}})-\Xi(\theta-\Theta_{\mathrm{(j-I)-}})\right]\Bigg\}.\end{aligned} \tag{17}$$

The Coulomb hysteresis amplitude $H(\theta)$ is written as the following piecewise linear function

$$H(\theta)=\sum_{\mathrm{j=I}}^{\mathrm{N}}\left\{\begin{array}{l}\left[H_{\mathrm{(j-I)+}}\left(\frac{H_{j+}-H_{\mathrm{(j-I)+}}}{\Theta_{j+}-\Theta_{\mathrm{(j-I)+}}}\right)\right]\left[\Xi(\theta-\Theta_{\mathrm{(j-I)+}})-\Xi(\theta-\Theta_{j+})\right]+\ldots\\ \quad\left[H_{\mathrm{(j-I)-}}\left(\frac{H_{\mathrm{(j-I)-}}-H_{\mathrm{j-}}}{\Theta_{\mathrm{(j-I)-}}-\Theta_{\mathrm{j-}}}\right)\right]\left[\Xi(\theta-\Theta_{\mathrm{j-}})-\Xi(\theta-\Theta_{\mathrm{(j-I)-}})\right]\end{array}\right\}. \tag{18}$$

Function $\Psi(\dot{\theta})$ is triple-valued and is defined as $\Psi(\dot{\theta})=\mathrm{sgn}(\dot{\theta})$.

The inertia parameters J_{A} and J_{B} are estimated by using a commercial solid modeling code [30]. The geometry of the torsion arm and shaft are measured to the nearest millimeter; material density is assumed to be uniform and estimated by measuring the mass of each component to the nearest 0.5 kg. Viscous damping ($C=2\zeta(JK_{\mathrm{III+}})^{0.5}$) is estimated by assuming a damping ratio of $\zeta=0.015$, which is typical for the torsional surge mode of a vehicle driveline [18]. The clearance transition $\Theta_{0\pm}$ is measured using a digital level [25] to the nearest 0.05°. All clutch damper parameters are estimated from measured quasi-static performance curves.

The non-linear model is numerically integrated using MATLAB [31]. The discontinuous functions $\Xi(\theta)$ and $\Psi(\dot{\theta})$ are approximated by the following smoothened functions where γ and η are empirical regularizing factors [32]

$$\Xi(\theta)\approx\hat{\Xi}(\theta)=0.5(\tanh(\gamma\theta)+1),\quad \Psi\left(\dot{\theta}\right)\approx\hat{\Psi}\left(\dot{\theta}\right)=\tanh\left(\eta\dot{\theta}\right). \tag{19a – b}$$

The maximum allowable time step for integration and the uniform output time step are chosen as τ_{s}. Three Runge–Kutta methods, of which one is intended for numerically stiff systems [31], are evaluated; however no significant difference among the results is found. A comparison of predicted and measured motions is given in Fig. 8 and Table 4. The simulated motions are characterized by the same response regimes as the measured signals. There is indeed very good agreement between the simple model and measurement for the DS regime and most of the SS regime. Nevertheless, the predicted

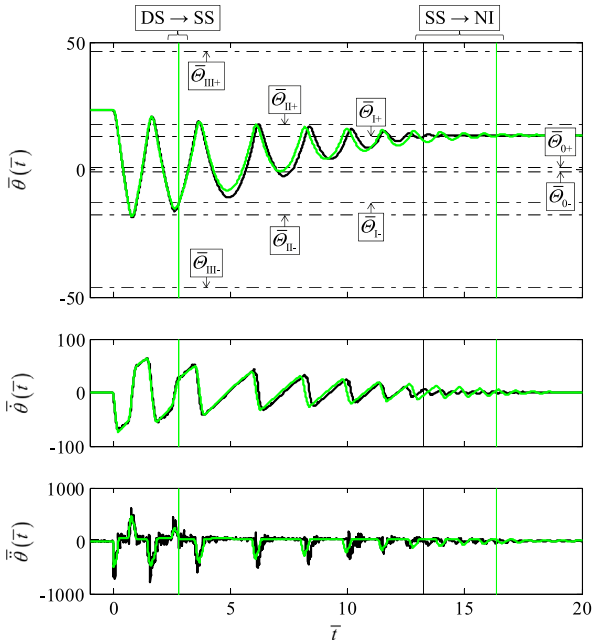

Fig. 8. Comparison of measured and predicted motions for $\bar{\theta}_{\mathrm{o}}\approx 23$ (with single clutch damper configuration). Key: (——) – measured motion, (|) – predicted motion using SDOF model, (|) – regime transition for the measured motion, (——) – regime transition for the simulated motion, (–•–) – stage and clearance transitions.

Table 4

Comparison of measured and predicted motions in terms of the mean (μ) and standard deviation (σ) of (a) peak-to-peak $\ddot{\overline{\theta}}(\overline{t})$ and (b) response regime transition times for $\overline{\theta}_o \approx 23$ (with single clutch damper configuration).

(a)	Peak-to-peak $\ddot{\overline{\theta}}(\overline{t})$ $(\mu \pm \sigma)$ for period					
Motion	1	2	3	4	5	6
Measured (over 12 sets)	802 ± 35	660 ± 19	541 ± 18	413 ± 9	342 ± 14	243 ± 15
Predicted	880	592	445	321	256	208

(b)	Response regime transition times $(\mu \pm \sigma)$	
Motion	$\overline{t}$(DS→SS)	$\overline{t}$(SS→NI)
Measured (over 12 sets)	2.94 ± 0.59	11.53 ± 0.50
Predicted	2.98	15.16

motions decay less quickly and the transition from SS to NI occurs much later. This suggests that the assumed dissipation model is insufficient and that further work would be needed to better quantify dissipation sources and refine $H(\theta)$.

7. Conclusion

The chief contribution of this article is the successful development of a new, refined vibratory (non-rotating) experiment that demonstrates the step response of a highly non-linear torsional system. This experiment differs from prior work [2,17–18] in that it includes multi-staged torsional stiffness and friction elements as provided by production clutch dampers. The experiment is conceptually designed using a SDOF torsional system model with discontinuous non-linear stiffness $K(\theta)$ and frictional hysteresis $H(\theta)$ which are assumed from quasi-static performance curves. To ensure relevance to vehicle powertrain subsystems and accuracy of measurement, a set of specific design objectives (such as the sizing for natural period, system actuation, instrumentation, and signal processing) are achieved. The angular motions are calculated from direct measurements of translational velocity (laser vibrometer) and translational acceleration (translational accelerometer). Typical measurements show that the step response is characterized by three pronounced non-linear regimes (DS, SS, and NI) which correspond to the multi-staged features of the clutch damper. Each measurement was quantified by two metrics: peak-to-peak $\ddot{\overline{\theta}}(\overline{t})$ and response regime transition times ($\overline{t}$(DS→SS) and $\overline{t}$(SS→NI)). The metrics for 12 measurements collected over three assemblies show that the results are repeatable. Calculation of $\overline{\theta}(\overline{t})$ is also verified by observing that all values of $\overline{\theta}_o - \overline{\theta}_f$ are within the tolerance of the directly measured values.

The predictions of a SDOF non-linear model exhibit the same qualitative nature as the measurements from the new experiment as both demonstrate the same non-linear response regimes, though there is only a partial agreement for the metrics. Therefore, this new experiment should provide time-domain benchmark data for the validation of higher dimensional non-linear models, while permitting an efficient process to evaluate the design of practical multi-staged torsional stiffness and friction devices. Even though a SDOF non-linear model is sufficient for experiment design and some predictions, further work is needed to develop better models as well as to extract dissipative parameters.

Acknowledgment

The authors acknowledge Eaton Corporation (Clutch Division) for supporting this research. We would like to thank Luiz Pereira and Brian Franke for their assistance with experimental studies. Further, we acknowledge the member organizations of the Smart Vehicle Concepts Center (www.SmartVehicleCenter.org) and the National Science Foundation Industry/University Cooperative Research Centers program (www.nsf.gov/eng/iip/iucrc) for partially supporting this basic research.

Appendix A. List of symbols

C torsional viscous damping
d pneumatic cylinder effective diameter
E modulus of elasticity
f frequency
g gravitational acceleration
H Coulomb hysteresis amplitude
J torsional inertia
K torsional stiffness

l	translational throw of the pneumatic cylinder
L	length
p	gauge pressure
t	time
N	number of clutch damper stages
T	torque
$u, \dot{u}$	measured translational displacement and velocity by laser vibrometer
$\ddot{v}$	measured translational acceleration by accelerometer V
$\ddot{w}$	measured translation acceleration by accelerometer W
x, y, z	translational coordinates
β	wave number
γ	displacement regularizing factor
ζ	damping ratio
η	velocity regularizing factor
$\theta, \dot{\theta}, \ddot{\theta}$	angular displacement, velocity, and acceleration
Θ	clutch damper stage transition (angular)
μ	arithmetic mean
Ξ	unit step function
ρ	material density
σ	standard deviation
τ	period
Ψ	signum function
ω	angular frequency

Subscripts

1, 2, 3	modal index
0, I, II...	clutch damper stage index
A	torsion arm
b	clearance
B	clutch shaft
D	clutch damper
e	external
j	index
f	final
max	maximum
n	natural
o	initial
r	rth mode
s	sampling
u	laser point
v	translational accelerometer V
w	translational accelerometer W
x, y, z	torsion arm dimension index
$+$	clutch damper drive side
$-$	clutch damper coast side

Superscripts

$-$	normalized
$\wedge$	estimated

Abbreviations

SDOF	single degree of freedom
ASM1, 2, 3	experiment assembly index
NI	no impact response regime
SS	single-sided impact response regime
DS	double-sided impact response regime

Appendix B. Specifications for instrumentation system

Polytec PSV-400 scanning laser vibrometer [22] and PSV-400-M4 data acquisition system [23]:

- Measurement range: $\pm$ 10 m/s
- Minimum sampling period: 1 μs
- Additional channels: 4

PCB translational accelerometer model 355B02 [25]:

- Sensitivity: 10 mV/g
- Measurement range: $\pm$ 500 g (peak)
- Frequency range for $\pm$ 5% accuracy: 1–10,000 Hz
- Frequency range for $\pm$ 10% accuracy: 0.6–12,000 Hz
- Frequency range for $\pm$ 3 dB accuracy: 0.3–17,000 Hz
- Resonant frequency: $\geq$ 35 kHz
- Broadband amplitude resolution (1–10,000 Hz): 0.0005 g RMS

PCB handheld shaker model 394C06 [24]:

- Operating frequency: 159.2 $\pm$ 1.6 Hz
- Acceleration amplitude: 9.81 $\pm$ 0.01 m/s^2 RMS
- Velocity amplitude: 9.81 mm/s RMS
- Displacement amplitude: 9.81 μm RMS

Craftsman Digital Torpedo Level [26]:

- Measurement range: 0–360°
- Accuracy of digital display: $\pm$ 0.1°
- Accuracy of vials: $\pm$ 0.029°

References

[1] F. Shaver, Manual Transmission Clutch Systems, SAE, 1997.
[2] P.H. Couderc, J. Callenaere, J. Der Hagopian, G. Ferraris, A. Kassai, Y. Borjesson, L. Verdillon, S. Gairmard, Vehicle driveline dynamic behavior: experimentation and simulation, J. Sound Vib. 218 (1) (1998) 133–157.
[3] C.L. Gaillard, R. Singh, Dynamic analysis of automotive clutch dampers, Appl. Acoust. 60 (2000) 399–424.
[4] W. Oh, R. Singh, Examination of clunk phenomena using a non-linear torsional model of a front-wheel drive vehicle with manual transmission, In: Proceedings of SAE Noise and Vibration Conference, Traverse City, MI, SAE Paper 2005-01-2291, 16–19 May 2005.
[5] L. Li, R. Singh, Analysis of vibration amplification in a multi-staged clutch damper during engine start-up, Proc. IMechE Part D: Journal of Automobile Engineering, 10.1177/0954407014563362.
[6] J.Y. Yoon, R. Singh, Effect of multi-stage clutch damper characteristics on transmission gear rattle under two engine conditions, Proc. IMechE Part D: J. Automob. Eng. 277 (2013) 1273–1295.
[7] R.A. Ibrahim, Recent advances in nonlinear passive vibration isolators, J. Sound Vib. 314 (2008) 371–452.
[8] J. Wang, R. Li, X. Peng, Survey of nonlinear vibration of gear transmission systems, Appl. Mech. Rev. 56 (3) (2003) 309–329.
[9] V.I. Babitsky, V.L. Krupenin, Vibration of Strongly Nonlinear Discontinuous Systems, Springer, Berlin, 2001.
[10] Y.S. Choi, S.T. Noah, Forced periodic vibration of unsymmetric piecewise-linear systems, J. Sound Vib. 121 (1988) 117–126.
[11] Y.B. Kim, S.T. Noah, Stability and bifurcation analysis of oscillators with piecewise-linear characteristics: a general approach, J. Appl. Mech. 58 (1991) 545–553.
[12] A.R. Crowther, N. Zhang, Torsional finite elements and nonlinear numerical modelling in vehicle powertrain dynamics, J. Sound Vib. 284 (2005) 825–849.
[13] A.R. Crowther, C. Janello, R. Singh, Quantification of clearance-induced impulsive sources in a torsional system, J. Sound Vib. 307 (2007) 428–451.
[14] M.D. Todd, L.N. Virgin, Natural frequency considerations of an impact oscillator, J. Sound Vib. 194 (1996) 452–460.
[15] M. Wiercigroch, V.W.T. Sin, Experimental study of a symmetrical piecewise base-excited oscillator, J. Appl. Mech. 65 (1998) 657–663.
[16] J. Ing, E. Pavlovskaia, M. Wiercigroch, Dynamics of a nearly symmetrical piecewise linear oscillator close to grazing incidence: modelling and experimental verification, Nonlinear Dyn. 46 (2006) 225–238.
[17] J.S. Gurm, W.J. Chen, A. Keyvanmanesh, T. Abe, A.R. Crowther, R. Singh, Transient clunk response of a driveline system: laboratory experiment and analytical studies, SAE Trans. J. Passeng. Cars: Mech. Syst. 116 (6) (2008). Paper # 2007-01-2233.
[18] A.R. Crowther, R. Singh, N. Zhang, C. Chapman, Impulsive response of an automatic transmission system with multiple clearances: formulation, simulation and experiment, J. Sound Vib. 306 (2007) 444–466.
[19] J. Wojewoda, A. Stefański, M. Wiercigroch, T. Kapitaniak, Hysteretic effects of dry friction: modelling and experimental studies, Philos. Trans. R. Soc. 366 (2008) 747–765, http://dx.doi.org/10.1098/rsta.2007.2125.
[20] D. Inman, Engineering Vibration, Pearson Education, Upper Saddle River, NJ, 2008.
[21] M. Serridge, T.R. Licht, Piezoelectric Accelerometer and Vibration Preamplifiers, Brüel & Kjær, Denmark, 1987.
[22] PSV-400 Scanning Vibrometer, Polytec Inc., ⟨http://www.polytec.com⟩ (accessed January 2015).
[23] PSV-400-M4 Data acquisition system, Polytec Inc., ⟨http://www.polytec.com⟩ (accessed January 2015).
[24] Handheld shaker, Model 394C06, PCB Piezotronics Inc., ⟨http://www.pcb.com⟩ (accessed January 2015).

[25] Translational accelerometer, Model 355B02, PCB Piezotronics Inc., ⟨http://www.pcb.com⟩ (accessed March 2015).
[26] Craftsman Digital Torpedo Level, ⟨http://www.sears.com⟩ (accessed March 2015).
[27] A.V. Oppenheim, R.W. Schafer, Discrete-Time Signal Processing, Prentice-Hall, Upper Saddle River, NJ, 1999.
[28] J.S. Bendat, A.G. Piersol, Random Data Analysis and Measurement Procedures, John Wiley & Sons, Hoboken, NJ, 2010.
[29] T.C. Kim, T.E. Rook, R. Singh, Effect of Impact damping on the frequency response characteristics of a torsional system, J. Sound Vib. 281 (2005) 995–1021.
[30] SolidWorks 3D CAD Design Software, Dassault Systemes, ⟨http://www.solidworks.com⟩ (accessed February 2015).
[31] MATLAB, MathWorks, ⟨http://www.mathworks.com/products/matlab/⟩ (accessed February 2015).
[32] T.C. Kim, T.E. Rook, R. Singh, Effect of smoothening functions on the frequency response of and oscillator with clearance non-linearity, J. Sound Vib. 263 (2003) 665–678.